Journal of Materials Science: Materials in Engineering

ORIGINAL PAPER

Open Access

Advancements in bandgap engineering: bromide-doped cesium lead perovskite thin films

Khawla Fradi[1,2,3*], Amal Bouich[3,4*], Yousaf Hameed Khattak[3,5*], Faisal Baig[3,5], Bechir Slimi[1], Bernabé Marí Soucase[3] and Radhouane Chtourou[1]

Abstract

Perovskite materials have emerged as promising candidates for next-generation photovoltaic devices due to their unique optoelectronic properties. In this study, we investigate the incorporation of bromine into cesium lead mixed iodide and bromide perovskites ($CsPbI_{3(1-x)}Br_{3x}$) to enhance their performance. By depositing films with varying bromine concentrations ($x = 0, 0.25, 0.5, 0.75$), we employ a combination of structural and optical characterization techniques, including X-ray diffraction (XRD), scanning electron microscopy (SEM), UV–visible spectroscopy, and photoluminescence. Our analysis reveals that introducing bromine leads to structural modifications, influencing the perovskite films' optical properties and energy gap. Specifically, we observe semiconductor behavior with a tunable energy gap controlled by the intercalation of bromine atoms into the $CsPbI_3$ lattice. Furthermore, heat treatment induces phase transitions in the perovskite films, affecting their optical responses and crystalline quality. SCAPS-1D simulations confirm the improved stability and efficiency of bromine-doped $CsPbI_3$ films compared to undoped counterparts. Our findings demonstrate that bromine incorporation facilitates the formation of highly crystalline perovskite films with reduced trap defects and enhanced carrier transport properties. These results underscore the potential of bromine-doped $CsPbI_3$ perovskites as promising materials for high-performance photovoltaic applications, paving the way for further optimization and device integration.

Keywords $CsPbI_{3(1-x)}Br_{3x}$, Film morphology, Stability, Bromide doping, Bandgap

Introduction

In recent years, researchers have focused on hybrid organic–inorganic perovskite-based solar cells; these perovskite materials have seen upward efficiency from 3.8% to over 25.2% in a short period (Jeong et al. 2020; Kim et al. 2021). In general, perovskite materials are in the form of ABX_3, A represents the organic cation, B is a metal, and the halogen is expressed by X (Bouich et al. 2021; Wang et al. 2022). Despite these perovskite solar cell hybrids exhibiting remarkable efficiency, these perovskite films are susceptible to degradation due to humidity and temperature conditions (Dunfield et al. 2020; Sutton et al. 2016; Liu et al. 2015). Significantly, the methylammonium lead iodide thin films thermally decompose to lead iodide at 100 °C (Fradi et al. 2022). Thermally, we find as results of

*Correspondence:
Khawla Fradi
khawlafradi@gmail.com
Amal Bouich
bouich.amal@gmail.com
Yousaf Hameed Khattak
yousaf.hameedk@gmail.com
[1] Laboratoire de Nanomatériaux et Systèmes pour les Energies Renouvelables, Centre de Recherches et des Technologies l'Energie, Technopole BorjCedria, Bp 95, Hammam-Lif 2050, Tunisia
[2] Faculté des Sciences de Tunis, Université d'El Manar, Tunis, Tunisia
[3] Institut de Disseny i Fabricació, Universitat PolitècnicaValència, Valencia, Spain
[4] Física Aplicada a las Ingenierías Aeronáutica y Naval & Instituto de Energía Solar Universidad Politecnica de Madrid, Madrid, Spain
[5] Electrical Engineering Department, Federal Urdu, University of Arts, Sciences & Technology, Islamabad, Pakistan

analyses in the literature that perovskites based on formamidinium are much less degradable than perovskites based on methylammonium, researchers tested a mixture of cations in the same perovskite film, it is an organic–inorganic mixture between formamidinium (organic cation) and cesium (inorganic cation), and they proved some thermal stability can exceed the value of 100 °C (McMeekin et al. 2016). From where comes The idea to enhance the stability of the thermal composition by thinking of partially changing the organic component with an inorganic cation, for example, the cesium element. Many studies have been carried out on the properties of lead cesium halides due to their excellent stability (Akkerman et al. 2018; Huang et al. 2020). Our work considers the two compounds, lead cesium bromide and cesium lead iodide, as a reference in our research. Both materials have slight stability up to the melting points. At room temperature, $CsPbBr_3$ reaches the crystallization phenomenon of the orthorhombic phase. It transitions to the tetragonal phase of perovskite at 87 °C and the cubic phase with orange color at 120 °C (Kulbak et al. 2015; Piotrowski et al. 2022). However, for $CsPbI_3$, a quick transition can occur to the yellow phase (δ phase) at temperatures below 315 °C, which does not absorb much sunlight. This problem was addressed by doping $CsPbI_3$ with other compounds to gain higher stability and better performance (Mir et al. 2019; Guvenc et al. 2019; Zhao et al. 2023). Under various conditions, black α-$CsPbI_3$ perovskites cannot reach their phase stability; this phase quickly changes to thermodynamically stable δ-$CsPbI_3$ (yellow color) in a short time, which has a non-perovskite structure and high bandgap for photovoltaic devices. Our idea is to prevent this phase transformation from taking advantage of the good properties of $CsPbI_3$. Various methods have been granted to inorganic perovskites to resolve this stability handicap; in this study, Br doping was used to increase the stability and improve the optical and structural properties of α-$CsPbI_3$. This idea leads to the surface passivation induced by the network modification, which causes stable perovskite nanocrystals under normal conditions (Bera et al. 2019; Lu et al. 2018). Besides,doping is the most widely used technique in various materials synthesis systems for different applications. After further research, experience shows that the reduction of the degradation phenomenon in perovskite materials is made under the effect of the deformation of the cubic phase. There was a decrease in the density of the defects and an increase in the tolerance factor of Goldschmidt (Fu et al. 2019). Thin film deposition of CsPbI3(1-x)Br3x is shown in Fig. 1

Manufacture of cesium lead mixed halide

Inorganic lead-based perovskites containing a bromine-iodine mixture were developed using different available precursors. Mainly, cesium iodide compounds (CsI), lead iodide (PbI_2), and lead bromide ($PbBr_2$) were applied and dimethyl sulfoxide (DMSO) and N, N-dimethylformamide (DMF) as stabilizing solvents. $CsPbI_{3(1-x)}Br_{3x}$ solution was spin-coated by centrifugation fluorine-doped tin oxide (FTO) substrate at 4500 rpm for the 30 s. The rapid vaporization of DMF/DMSO causes disturbances on the surfaces of the samples; to overcome this drawback, four to five drops of toluene are added, while the substrate is rotating on the spin coating; the addition of toluene produces optimal morphology and good crystallinity. Also, the injection of toluene must be rapid and not drop by

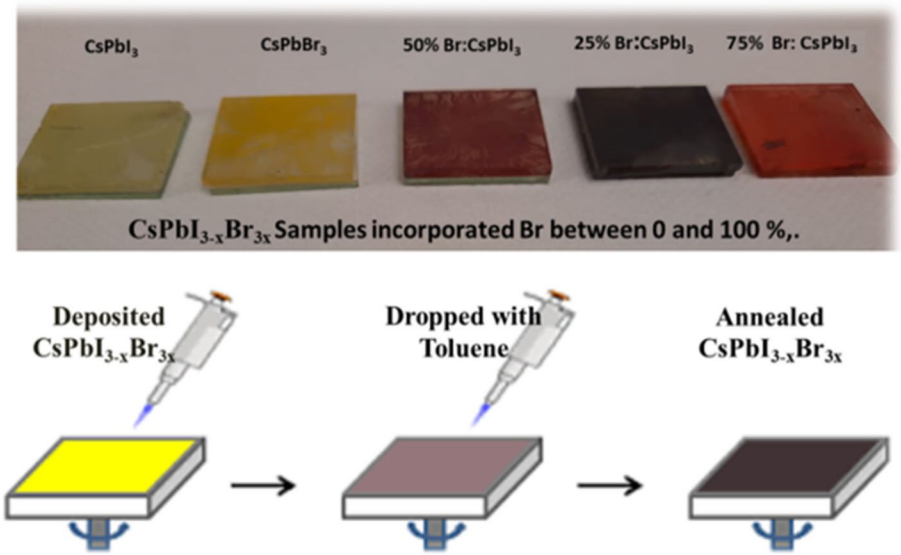

Fig. 1 Thin film deposition of $CsPbI_{3(1-x)}Br_{3x}$

drop because it causes poor morphology and crystallinity. For 5 min, the transparent thin films were heated at a low temperature (slow thermal heating), 70 °C, which transformed from yellow to orange depending on the bromine's addition concentration. After successful deposition, these thin films were subjected to surface morphology, optical bandgap, and structure characterization. But before conducting these studies, we reheated the same series of films on the heating plate at 180 °C for a structural and optical study for 10 min. During this reheating time, it is noticed that the films gradually take on a darker color by removing any remaining solvent. The appearance of a darker shade of the film proves the complete formation of the perovskite phase during annealing.

Characterization techniques

The X-ray diffraction is used with the Cu ka radiation ($k=1.5418$ A°) of Rigaku Ultima IV to characterize the $CsPbI_{3(1-x)}Br_{3x}$ thin films. The morphology of the films was characterized using scanning electron microscopy (Quanta 200—FEI) with 1.5-kV capture conditions at different magnifications. The measurements of absorption and transmission were taken by an Ocean Optics HR4000 spectrophotometer (Si-CCD) in the range of 350-nm and 850-nm wavelengths. We did the photoluminescence measurements using the He-Cd laser source emitting at 325 nm, and we detected the photoluminescence emissions by a back-thinned Si-CCD detector (Hamamatsu).

Results and discussions

X-ray diffraction analysis

The structural characteristics of $CsPbI_3$ and $CsPbI_{3(1-x)}Br_{3x}$ films by X-ray diffractograms are exhibited in Fig. 2. It was identified that for the α-$CsPbI_3$ phase, many XRD peaks are assigned to the (110) planes, (110), (200), and (211), corresponding to angles at 14.6°, 20.7°, 31.1°, and 33.28° (JCPDS, 01–075-0412). A slight shift at the peaks towards the lower angles after the intercalation of Br in thin films of $CsPbI_3$ is remarkable; the large size of bromine relative to the iodine halide is the cause of this transformation. The peak located at 12.8° is the peak that indicates the appearance of the undesirable δ-$CsPbI_3$ phase (Fig. 2). Furthermore, the integration of Br substance from (0–100%) the secondary phaseδ-$CsPbI_3$ gradually disappears and changes to the desired α-$CsPbI_{3(1-x)}$ Br_{3x} perovskite structure. For $CsPbI_{3(1-x)}Br_{3x}$ ($x=0$, 0.5) perovskites, a peak close to 13° appears which explains the non-perovskite phase of $CsPbI_3$, whereas for $CsPbI_{3(1-x)}Br_{3x}$ ($x=0.25$), this peak no longer exists. We conclude that the film doped with 25% bromine shows some compositional stability under the same conditions. The shift of XRD peaks to higher angles is noticed during the doping procedure. This change can prove that the doping process is taking place accurately in the perovskite structure. Because of the smaller ionic radius of the brome halide (115 pm) than the iodide halide (140 pm), peaks shift to higher angles. Another fundamental remark in the XRD model that has been noticed is the division of the peak of (200) for the sample $CsPbI_{3(1-x)}Br_{3x}$ ($x=0.25$); the division can be done by scaled-down symmetry in the cubic structure perovskite. A prolongation of stability may occur in the α phase due to lattice distortion. The ionic radius of bromine is smaller than the ionic radius of iodine. Concerning the Goldschmidt tolerance factor (Eq. 1) (Bouich et al. 2022), it is improved under the effect of the intercalation of bromine, which has a size of the ionic radius smaller than the ionic radius of iodine. In the perovskite structure, the radius of the site A cation is presented by R_A, R_B expresses the radius of the site

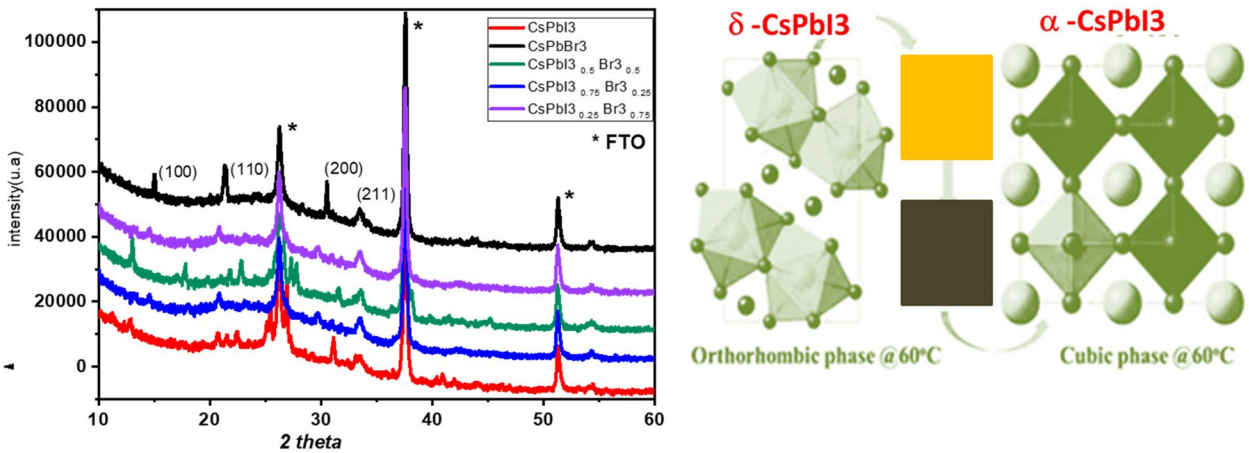

Fig. 2 XRD patterns for varying bromine content in $CsPbI_{3(1-x)}Br_{3x}$ films

B cation, and R_X marks the radius of the anion (Bouich et al. 2022).

$$t = (R_x + R_A)/\sqrt{2}(R_x + R_B) \quad (1)$$

Tolerance factor calculation

Taking our case of doping, the calculation of the influential tolerance factor is done using the formulas in Eq. 2.

For ordered double perovskites of the $AB(X'X)_3$ type with two different halogens in the X sites, since the tolerance factor relationship is applicable to both single and double perovskites, the Goldschmidt factor can be calculated by replacing the bond length ***B***-X bond length in the case of the single perovskite by the average of the bond lengths bonds < ***B***-X, ***B***-X′ > to give the following (Bouich et al. 2022):

$$R'x = (R_{I-} + R_{Br-})/2 \quad (2)$$

$$R' = \left(R'x + R_A\right)/\sqrt{2}\left(R'x + R_B\right) \quad (3)$$

Influence of bromine doping on film stability

The influential tolerance factor also increased when bromine was introduced into the $CsPbI_3$ perovskite structure. The increase in this factor translates into a more stable perovskite structure. In our work, we have guaranteed the stability of $CsPbI_{3(1-x)}Br_{3x}$ compound since the further the Goldschmidt factor deviates from 1.1, the more deformed the lattice becomes. It has usually been believed that a suitable range for perovskite is 0.8–1.10 (Table 1) (Bouich et al. 2022).

Table 1 Effect of bromine additive on tolerance factor in $CsPbI_3$ perovskites

Sample	*R′*x (nm)	*t′*: tolerance factor
$CsPbI_3$	0.140	0.85
$CsPbI_{3(1-x)}Br_{3x}$ ($x = 0.5$)	0.127	0.86
$CsPbBr_3$	0.115	0.87

Scanning electron microscopy (SEM) analysis

However, the structural and morphological response of films based on $CsPbI_3$ and $CsPbBr_3$ is unsatisfactory due to the poor quality of perovskite thin films. In this situation, by combining both substrates with preheat treatment $CsPbI_{3(1-x)}Br_{3x}$ and the additive precursor of bromine, we composed the high-quality $CsPbI_{3(1-x)}Br_{3x}$perovskite film, giving full coverage, excellent crystallinity, and high crystal grain size, which improves the light collection and weakens non-radiative charge recombination. The SEM images picked up from thin films of perovskite with intercalation of the halide Br and the pure compound $CsPbI_3$ are shown in Fig. 3.

The perovskite film obtained reveals poor morphology with nonhomogeneous coverage and low crystallinity without adding bromine. However, the $CsPbI_{3(1-x)}Br_{3x}$ film shows full substrate coverage without voids and crystal grains of large sizes. It offers that the combination of bromine and iodide significantly affects the construction of the perovskite film morphology, in good agreement with the literature (Guo et al. 2019; Wang et al. 2020).

SEM images are shown in Fig. 3; we note that for pure $CsPbI_3$ substrates, several holes appear on the surface, indicating a specific magnification at the level of the surface morphology. The 25% Br sample shows excellent morphology, which agrees with the results of the XRD,

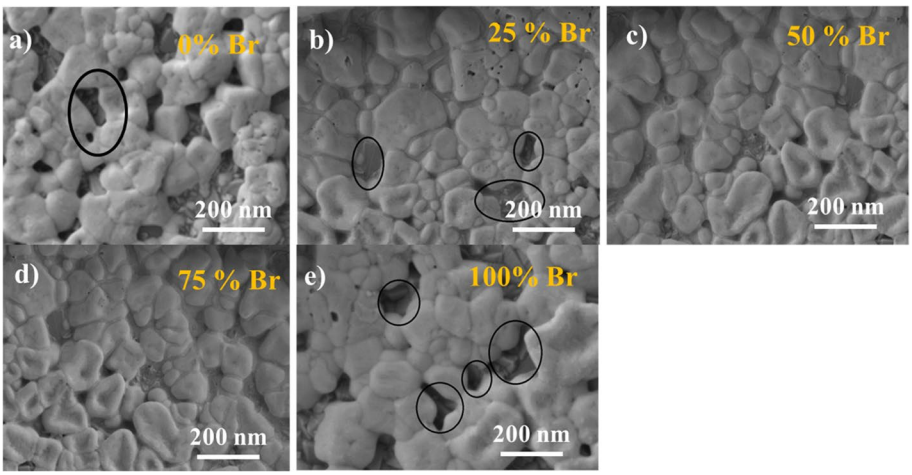

Fig. 3 Top-view SEM analysis of $CsPbI_{3(1-x)}Br_{3x}$ films with **a** 25%, **b** 50%, and **c** 75% of bromine

and PL-confirmed stability against the pure $CsPbI_3$ thin film. Besides, substituting the halide Br content stabilizes the yellow phase of $CsPbI_3$ with enhanced XRD, suppressing the undesirable perovskite phase transition.

Optical properties analysis

Adding the amount of Br camouflages the diffuse absorption of the pure $CsPbI_3$. Also, the absorption edge observed a remarkable enhancement at the highest energy wavelength. Furthermore, one sharp peak was observed in the 500–600 nm range in Fig. 4, possibly because of absorbent materials' electronic transition, rotational, or vibrational energy levels. This information is consistent with the increase in crystallinity in the results of the XRD. The bandgap is measured by the Tauc method, illustrated in Fig. 5.

Photoluminescence spectra analysis

The present study reports the optical characteristics of cesium perovskites based on lead and halides. $CsPbI_{3(1-x)}Br_{3x}$ ($X=0$, 0.25, 0.5, 0.75, 1). The computed optical structure profile proves that these materials

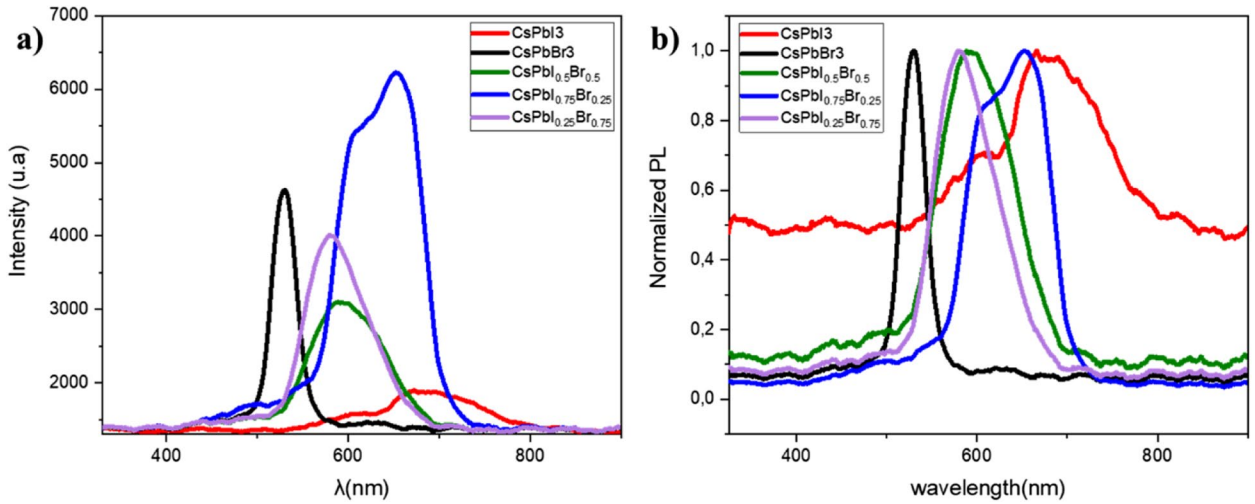

Fig. 4 **a** Photoluminescence variation in $CsPbI_{3(1-x)}Br_{3x}$ films. **b** Normalized photoluminescence spectra of $CsPbI_{3(1-x)}Br_{3x}$ films

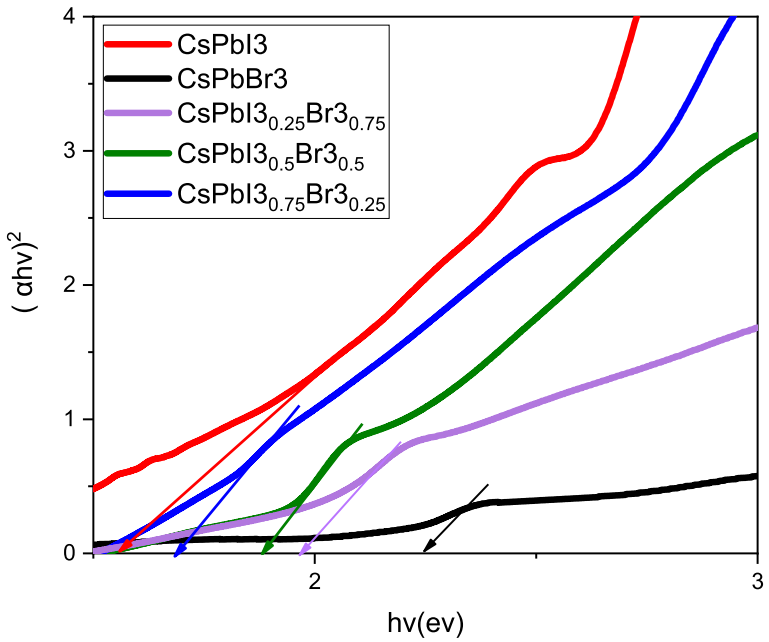

Fig. 5 Band gap variation with bromine content in $CsPbI_{3(1-x)}Br_{3x}$ perovskites

expose semiconductor behavior with a photoluminescence value of $CsPbI_3$ regulated by the intercalation of an atom of bromine by an atom of iodine in $CsPbI_3$.

Bromine belongs to the same column as iodine in the periodic table, so they have properties in common. The elements to which they belong have the same number of electrons on their outer layer, which gives them similar properties, and it is this outer layer that is responsible for their similar reactivity.

Our work is to understand the ionic transport mechanism by introducing suitable halogen substitution with insignificant impact on perovskite photoluminescence value to hinder ion diffusion and thereby to seek a method to improve the stability. The research results show that a bromine substitution not only prevents ion migration in perovskite but also promotes the intensity of photoluminescence; this result is very clear in the example. In Fig. 4, the strong absorption at 660 nm corresponds to the perovskite $CsPbI_{3(1-x)}Br_{3x}$ ($x=0.25$). Furthermore, smaller atomic substitution for the halogen atoms may be essential for increasing the diffusion barrier. Bromine doping can also introduce defects into the perovskite crystal structure. These defects can act as recombination sites for charge carriers, which reduces the efficiency of photoluminescence; this interpretation explains the increase in the values of the widths at half maximum, at the level of the perovskites doped with bromine, and also at the level of the peak which corresponds to the value 660 nm where we note that the intercalation of bromine can also form complexes with the perovskite, which can modify the photoluminescence properties of the material. We suggest that partial bromine substitution is beneficial for the $CsPbI_3$ perovskite to have the most intense peak of photoluminescence, although none of the substitutions has better optical proprieties than lead iodine perovskite with 25% of bromine does currently.

Bandgap variation with bromine content

The bandgap energies have decreased to the lower point with Br from 100 to 0%. In our case, incorporating 25% Br content reinforced the lattice parameter changes proposed in the previous section.

Table 2 explains the values of the optical bandgap (Eg) of $CsPbI_{3(1-x)}Br_{3x}$, removed from PL and UV measurements. When adding the bromine amount assay, the absorption limit decreased significantly from 2.24 to a value of 1.68 eV. The overall difference in PL emission between the $CsPbI_3$ and $CsPbI_{3(1-x)}Br_{3x}$ samples is from 2.34 to 1.7 eV. The bandgap measurements of $CsPbI_{3(1-x)}Br_{3x}$ substrates are characterized in a typical environment after 1 week called aged thin films. The recovered samples' band gap value was fixed ~ 2 times less than the sample characterized a week later. In the air, the improvement in absorbance can be attributed to the creation of vacancies under the effect of the intercalation of Br in the $CsPbI_3$ network. Charge recombination is decreased by lowering surface trap states, leading to increased photoelectric efficiency.

Table 2 Band gap tuning in $CsPbI_{3(1-x)}Br_{3x}$ films

Sample ID	PL-Eg (eV)	UV-Eg (eV)	Stokes shift (eV)
0% of Br	1.7	1.68	0.02
25% of Br	1.89	1.78	0.11
50% of Br	2.01	1.88	0.13
75% of Br	2.14	1.96	0.18
100% of Br	2.34	2.24	0.10

Figure 4a and b confirms the growth of the spectra of emission, which correspond to $CsPbI_3$ varying the percentage of Br ($x=0\%$, 25%, 50%, 75%, and 100%). An apparent change was noted in the normalized photoluminescence spectrum at the lowest wavelengths. This wavelength deviation proves the assembly of I_3/Br_3 in the perovskite latticework. The number of non-radiative emissions decreases, which results in a reduction in the level of the density of states of the traps; this result is explained in the amplified emission spectrum of PL. The transformation of pure $CsPbI_3$ to the mixed material $CsPbI_{3(1-x)}Br_{3x}$ was noticed in the photoluminescence spectra; this result is in good agreement with the results of the X-ray and absorption spectra. In summary, Table 2 summarizes the responses of the photoluminescence spectra and visible UV spectroscopy of $CsPbI_3$ for different Br_3 contents. In Table 2, we can conclude that for 25% of Br_3, the value of the gap energy of $CsPbI_{3(0.75)}Br_{3(0.25)}$ is smaller compared to the value of the bandgap of $CsPbBr_3$, which the intercalation of Br can explain, and then the creation of one more energy space between the valence and the conduction band, and consequently to the reduction of the gap.

It can be noted that $CsPbI_3$ has a higher absorbance value than $CsPbBr_3$, science explains the variation of the value of the bandgap by the phenomenon of absorption in the visible range, and it is an internal characteristic for each type of material, which causes a weakening of the energy of the bandgap due to the quantities adding bromine content.

The halide is the most crucial element of hybrid perovskites, the atomic size increases by descending in group VIIA from the chloride halide to the iodine, the changed absorption spectrum translates to longer wavelengths, and a decrease in energy occurs as the absorption spectrum moves toward the highest wavelengths,

i.e., a redshift is created (Jeong et al. 2021); the reduction can explain this in electronegativity to have such compatibility with lead, increasing the covalency and effectively minimizing the ionic character. Bromide was most profitably used to adjust the bandgap hybrid perovskites (Lu et al. 2021). Iodide is the closest lead on the periodic table, so it shares a similar covalent character, which leads to a similar covalent character to form a stable structure.

When Br is included in $CsPbI_3$, compression stress between Pb–I bonds is introduced due to the size of the lattice parameters, leading to a structural distortion that causes an increase in the bandgap value (Appadurai et al. 2021). For our case, Fig. 5 confirms that the bandgap value of $CsPbI_{3(1-x)}Br_{3x}$ was limited from 1.6 ($CsPbI_3$) to 2.1 eV ($CsPbBr_3$). An adequate amount of 25% of bromine intercalated in $CsPbI_3$ was confirmed by the results with a slow annealing treatment guide to successfully synthesize perovskite films with large absorbance and bandgap equal to 1.65 eV.

Degradation study

Making the balance between the high-power conversion efficiency and the stability of hybrid perovskite solar cells is challenging to commercialize solar cells. For this reason, the value of the bandgap is the secret to the physical conversion process in the photovoltaic field; the optical response of organic–inorganic hybrid perovskite would change by its properties and the environmental situations, like temperature and pressure, which affected directly the stability of perovskite solar cells (Sun et al. 2017). This part will cover the stability under a thermal condition, like in our case, the relation of the optimization of the bandgap with the temperature to give a complete overview of the phenomenon of the degradation of perovskite by exposing it to the air for a week. However, research has explored $CsPbX_3$ compounds as photovoltaic materials. Still, α-$CsPbI_3$ thin films undergo an abrupt orthorhombic phase change. Oxygen and humidity are the most direct factors affecting photovoltaic stability. We aim to study the degradation phenomenon of $CsPbI_{3(1-x)}Br_{3x}$ films deposited using heat treatment. Perovskite thin films were protected in the dark at room temperature for 1 week. After 1 week, to examine the degradation of samples, we reheated the perovskite films on the heating plate at 180 °C for 10 min. We studied the optical response of the samples under reheating. Molecules of H_2O present in the air lead to the degradation of the films. They probably cause the breaking of the bonds between the synthesized mixed perovskite molecules and end with a change of the film color and appearance of a non-perovskite phase. In addition, in Fig. 6d, after a week in which the $CsPbI_3$ film is exposed to air and humidity, the curve shows that the energy of the $CsPbI_3$ material obtained is equal to 3.3 eV; this result indicates that the phase is degraded. It does not correspond to a perovskite phase.

On the other hand, we notice the appearance of the two phases by analyzing Fig. 6c, where the film is reheated at 180 °C. Figure 6a and b shows the UV–visible absorption spectra of the aged and recovered perovskite films to quantify the stability of films and the effect of temperature on the absorption and the bandgap of different concentrations added of bromine. It can be seen that the absorption is greater with increasing iodide contents. At the same time, similar absorption bandgaps were exhibited, suggesting that the addition of iodide and the idea of synthesizing a mixed compound can enhance the light absorption properties since the pure $CsPbBr_3$ compound has the lowest absorption band. For aged films, after 1 week, we noticed that the absorption range was lower than in recovered films; this result convinced us to admit that optical treatment has a nice effect on the absorbent surface of perovskite. By comparing the value of the bandgap from estimating the optical band gap via fitting the experimentally determined absorption coefficient from Tauc equation, we note that for the aged $CsPbI_{3(1-x)}Br_{3x}$ ($x=0.25$), Eg = 1.73 eV, while for the recovered $CsPbI_{3(1-x)}Br_{3x}$ ($x=0.25$), Eg = 1.65 eV.

Encouragingly, the photoluminescence spectrum response and the optical characterization of the pure material containing Br significantly improve film performance and stability. The 25% Br is critical in slowing down the poor quality of $CsPbI_3$ thin films. Certain optical characterization techniques can indeed accelerate the degradation of perovskite materials. This happens due to several factors like light exposure, and perovskites can be sensitive to light, particularly high-energy photons like UV light. Techniques like photoluminescence (PL) spectroscopy involve excitation by light, which can induce photodegradation processes. Additionally, some optical methods, like those using focused laser beams, can generate localized heating. This heat can accelerate chemical reactions within the perovskite, leading to degradation. The degradation can be also explained by ambient factors, and exposure during characterization can introduce the perovskite to ambient air or moisture, which can also contribute to degradation. Researchers minimize these degradation effects by using low-powered light sources, pulsed lasers to minimize heat generation, and performing measurements in inert atmospheres.

As a result, the study of absorbance spectroscopy has improved the degradation of the perovskite layers. The apparent color of the film is related to the growth stages of the perovskite layer, which begins to darken at the

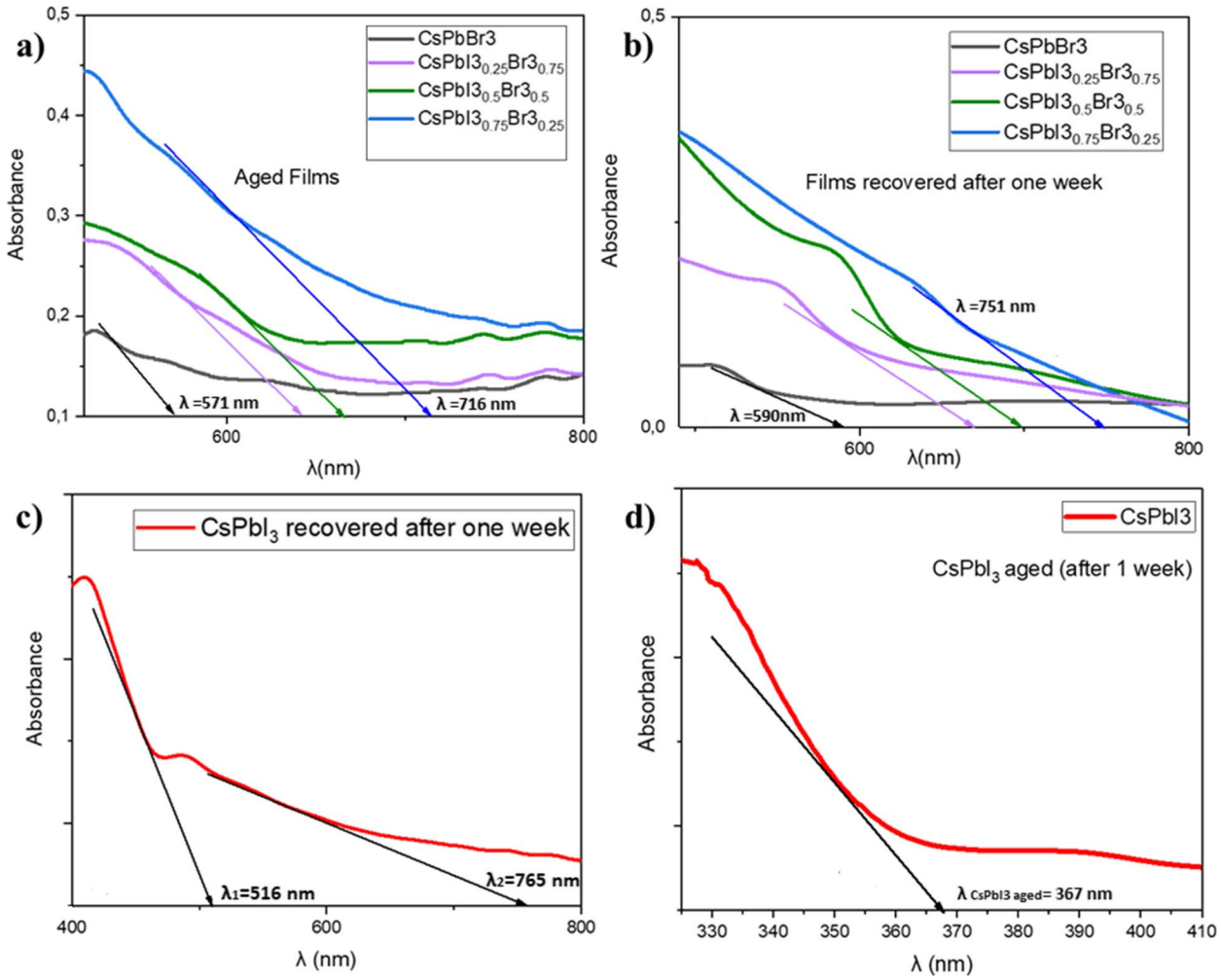

Fig. 6 Variation of absorbance in aged vs. recovered $CsPbI_{3(1-x)}Br_{3x}$ films across bromine concentrations

beginning and then changes to brown a week later, as visible in the photo (Fig. 7).

SCAPS simulation

The results of the degradation study effect after Br doping on $CsPbI_3$ were further investigated by simulating a device structure in SCAPS that incorporates band gap variation along with a change in absorption profile for the device. There are various ways to analyze these results as there is no limitation to the structure of the device because $CsPbI_3$ can be utilized as an absorber layer or $CsPbBr_3$ due to its wide bandgap can be used as a hole transport layer (HTL) (Chen et al. 2020; Yadav et al. 2023). But however, in this work, we used the fabricated layer properties as an intermediate layer between the absorber layer and HTL. The device structure that was simulated in SCAPS-1D is given as TiO_2/$MAPbI_3$/$CsPb(I,Br)_3$/Spiro-MeOTAD. The physical parameters for the device are given in Table 3.

First, the device was simulated for as-deposited samples of $CsPbI_3$ doped with different concentrations of Br by incorporating as-deposited band gap values and absorption profiles for the samples. The results for as-deposited samples are shown in Fig. 8. From Fig. 8, it is evident that the device that is doped 25% with Br shows the highest power conversion efficiency (PCE%). The reason for this is that it has a good band alignment with the absorber and HTL layer, as discussed in detail in our previous work (Bouich et al. 2022). But if we look at the inset table of the figure, there is no big difference in PCE for all Br-doped intermediate layers on the performance of solar cells.

However, after simulating samples, it was observed in SCAPS-1D that there is a variation in the performance of solar cells. The results of the degradation of the device are shown in Fig. 9. From Fig. 9, it is evident that we are not able to get the results for the pure $CsPbI_3$ sample, and the main reason for this is its bandgap

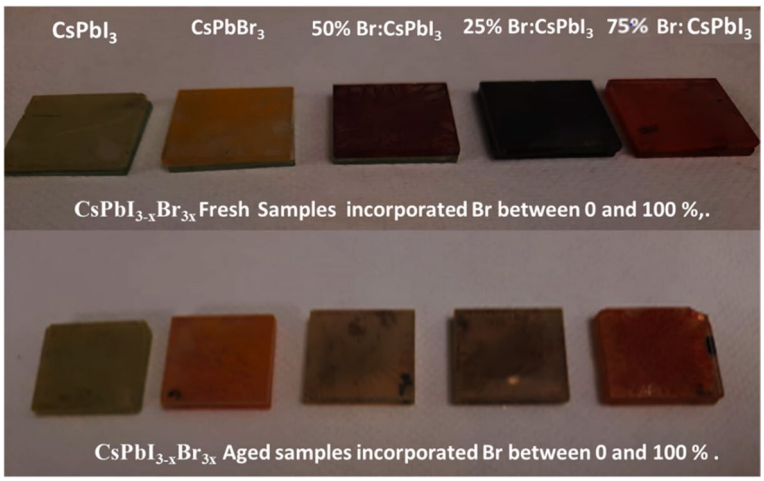

Fig. 7 Degraded samples $CsPbI_{3(1-x)}Br_{3x}$ with 0% and 25%, 50%, and 75% and 100%

Table 3 Physical parameters for device structure (Bouich et al. 2022, 2023; Sonmezoglu and Akin 2020; Akman et al. 2023, 2021; Baig et al. 2020; Motta et al. 2015; Khattak et al. 2022, 2021, 2020, 2023; Marí Soucase et al. 2022)

Parameters	Spiro MeOTAD	*MAPbI3*	*CsPbI3*	*TiO2*
E_g (eV)	3	1.55	Experimental values	3.2
χ (eV)	2.2	3.9	3.2 ~ 3.4	4
ε_r	3	10	10 ~ 7.3	9
N_c (cm^{-3})	1×10^{19}	2.8×10^{18}	2.8×10^{18}	1×10^{19}
N_v (cm^{-3})	1×10^{19}	3.9×10^{18}	3.9×10^{18}	1×10^{19}
n, p (cm^{-3})	1×10^{18}	1×10^{16}	1×10^{18}	1×10^{16}
μ_e (cm^2 / Vs)	50	11.8	270	20
μ_p (cm^2 / Vs)	50	11.8	270	10

w thickness, E_g bandgap, χ electron affinity, ε_r dielectric permittivity, N_c, N_V density of states, μ_e, μ_p carrier mobility, *n*, *p* carrier concentrations

got much wider, thus creating a large band offset in between the absorber and HTL layer, which SCAPS-1D is not able to simulate. In contrast, there is an overall reduction in PCE of the device.

After applying the profiles recovery stage on Br-doped $CsPbI_3$ samples, results for bandgap and absorption profile were again incorporated in the SCAPS-1D environment to analyze how the recovery of samples plays a role in device performance. After incorporating these results, we found out that devices doped with Br showed a slight increase in device performance, and this is shown in Fig. 10, whereas a comparison was also drawn in Table 4. From Table 4, one can deduce that undoped $CsPbI_3$ faced degradation at a higher rate than that of doped samples.

Table 5 below summarizes the different values of the optical bandgap (Eg) of $CsPbI_{3(1-x)}Br_{3x}$ by comparing our work with the results found in the literature. A comparative analysis between the results of our experiment and those of other research allows us to conclude on the validity of our hypotheses. The knowledge constructed through experimentation is supplemented by the confirmation of results similar to our values obtained.

This work aimed to propose and study the potential of substituting a quantity of bromine in $CsPbI_3$ perovskites which will be ready for use in solar cells with a well-optimized gap value. The work focused mainly on the composition of alloys of the $CsPbI_{3(1-x)}Br_{3x}$ type via changing the molar ratio of the precursors. After comparing our results with numerical and theoretical findings in existing studies, we have successfully created halogenated hybrid perovskites. These materials have been combined with other layers in solar cells. This breakthrough suggests a coming revolution in solar technology that could greatly enhance the efficiency of traditional solar cells.

Conclusion

In summary, we report a strategy induced by the institution of bromine to prepare $CsPbI_{3(1-x)}$ Br_{3x} inorganic perovskite films. By combining the two compounds CsBr and CsI as the main precursors of synthesis, highly crystalline $CsPbI_{3(1-x)}Br_{3x}$ ($x = 0$, 0.25, 0.5, 0.75) films are obtained via crystal rearrangement after annealing. In our article, the optimization of the amount of bromine addition in perovskite-based solar devices $CsPbI_3$ may well increase yield since it provides self-passivation at the grain boundaries and uniform grain sizes, which weakens the potential barrier between the crystal and the grain

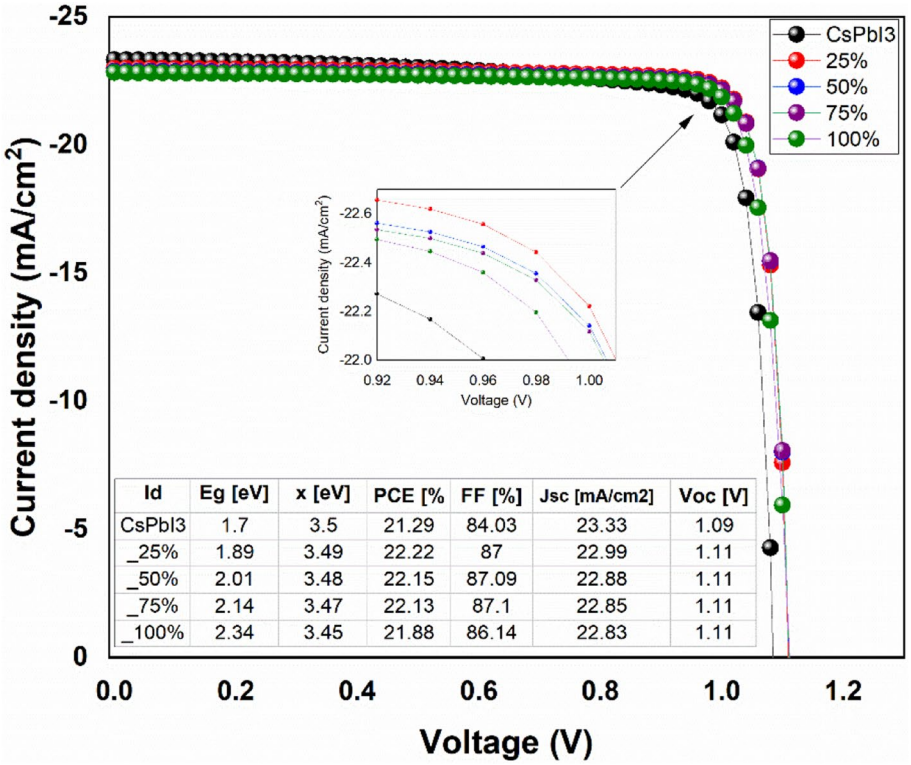

Id	Eg [eV]	x [eV]	PCE [%	FF [%]	Jsc [mA/cm2]	Voc [V]
CsPbI3	1.7	3.5	21.29	84.03	23.33	1.09
_25%	1.89	3.49	22.22	87	22.99	1.11
_50%	2.01	3.48	22.15	87.09	22.88	1.11
_75%	2.14	3.47	22.13	87.1	22.85	1.11
_100%	2.34	3.45	21.88	86.14	22.83	1.11

Fig. 8 As deposited CsPbI3-doped samples

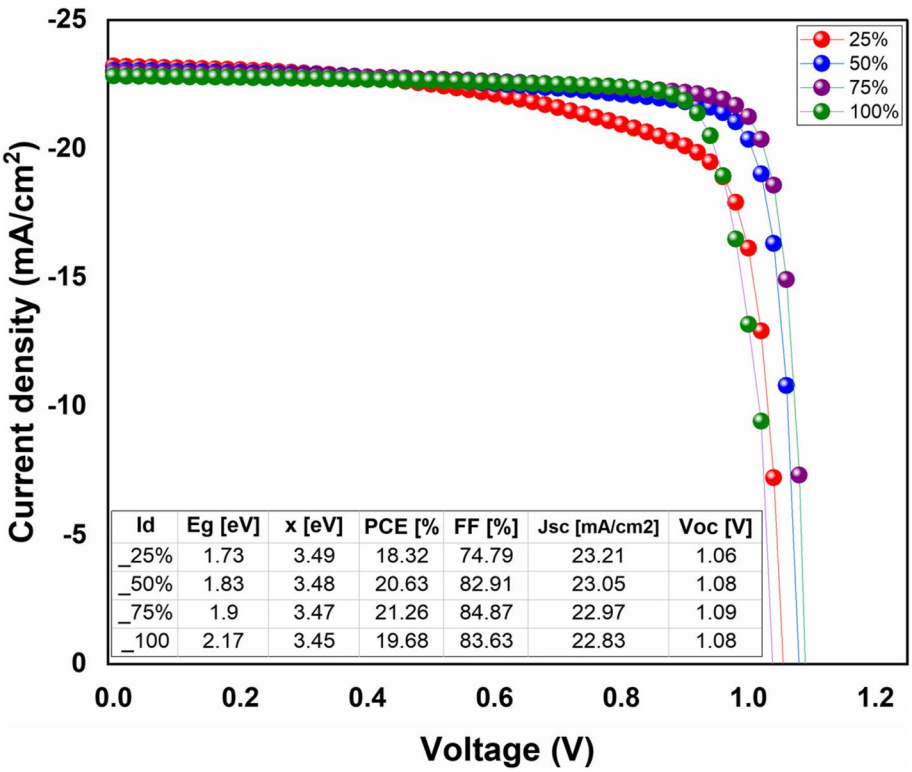

Id	Eg [eV]	x [eV]	PCE [%	FF [%]	Jsc [mA/cm2]	Voc [V]
_25%	1.73	3.49	18.32	74.79	23.21	1.06
_50%	1.83	3.48	20.63	82.91	23.05	1.08
_75%	1.9	3.47	21.26	84.87	22.97	1.09
_100	2.17	3.45	19.68	83.63	22.83	1.08

Fig. 9 Degradation of Br-doped $CsPbI_3$ samples

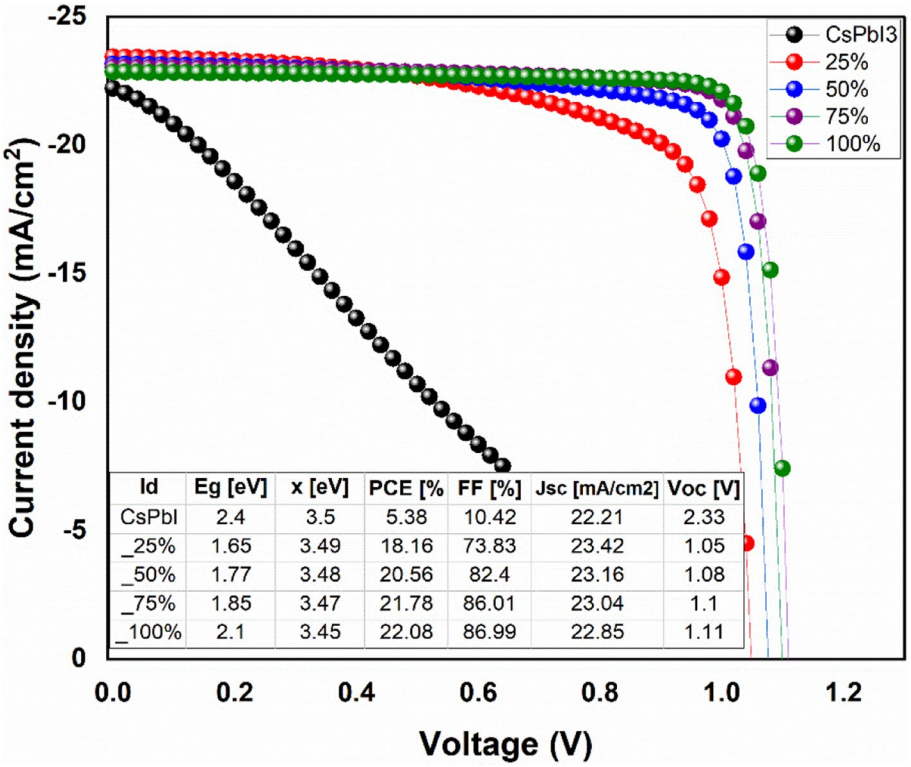

Fig. 10 Recovery stage on Br-doped $CsPbI_3$ samples

Table 4 Comparison table

Samples		Efficiency [%]			
	***CsPbI*$_3$ undoped**	**25% of Br**	**50% of Br**	**75% of Br**	**100% of Br**
As-deposited and doped $CsPbI_3$	21.29	22.22	22.15	22.13	21.88
Degradation of $CsPbI_3$ and Br doped	No result	18.32	20.63	21.26	19.68
Recovery stage of $CsPbI_3$ and Br doped	5.38	18.18	20.56	21.78	21.28

Table 5 Comparative table of results

SampleID	Experimental result of Eg (eV)	Numerical result of Eg (eV)	Theoretical result of Eg (eV)
0% of Br	1.7	1.75 (Jeong et al. 2021)	1.73 (Jeong et al. 2021)
$CsPbI_xBr_{3-x}$	1.89	1.69 to 2.3 eV (Jeong et al. 2021)	1.73 to 2.3 eV (Jeong et al. 2021)
100% of Br	2.34	2.3 (Jeong et al. 2021)	2.4 (Jeong et al. 2021)

boundary and minimizes trap defects; the purpose is to facilitate carrier transport. These results are well aligned with our SCAPS-1D simulation work, which clearly shows that samples that are doped with Br have higher recovery and efficiency than undoped samples.

Acknowledgements
The author Amal Bouich, a postdoctoral researcher, acknowledges Margarita Salas Fellowship (MCIN/AEI/10.13039/501100011033) for funding support. This work was supported by the EU under project PID2019-107137RB-C22 and by ERDF under the funding "A way of making Europe." This work was supported by the Ministerio de Ciencia e Innovación through the project BESTMAT-QC (PID2019-107137RB-C22).

Authors' contributions
KF, AB, BS, and RC contributed to conceptualization and methodology. KF, BS, and RC were responsible for data curation and formal analysis. BMS supervised the research. KF, AB, YHK, and BMS provided critical review and editing for the manuscript. YHK, FB, and BMS contributed to work on software and investigations.

Availability of data and materials
Not applicable.

Declarations

Ethics approval and consent to participate
Not applicable.

Competing interests
The authors declare that they have no competing interests.

Received: 15 April 2024 Accepted: 17 July 2024
Published online: 05 August 2024

References

Akkerman QA, Abdelhady AL, Manna L (2018) Zero-dimensional cesium lead halides: history, properties, and challenges. J Phys Chem Lett 9:2326–2337. https://doi.org/10.1021/acs.jpclett.8b00572

Akman E, Shalan AE, Sadegh F, Akin S (2021) Moisture-resistant FAPbI 3 perovskite solar cell with 22.25 % power conversion efficiency through pentafluorobenzyl phosphonic acid passivation. Chemsuschem 14:1176–1183. https://doi.org/10.1002/cssc.2020027075

Akman E, Ozturk T, Xiang W, Sadegh F, Prochowicz D, Tavakoli MM, Yadav P, Yilmaz M, Akin S (2023) The effect of B-site doping in all-inorganic CsPbI x Br 3–x absorbers on the performance and stability of perovskite photovoltaics. Energy Environ Sci 16:372–403. https://doi.org/10.1039/D2EE01070D

Appadurai T, Kashikar R, Sikarwar P, Antharjanam S, Nanda BRK, Chandiran AK (2021) Manipulation of parity and polarization through structural distortion in light-emitting halide double perovskites. Commun Mater 2:68. https://doi.org/10.1038/s43246-021-00172-9

Baig F, Khattak YH, Shuja A, Riaz K, Soucase BM (2020) Performance investigation of Sb2Se3 based solar cell by device optimization, band offset engineering and Hole Transport Layer in SCAPS-1D, Curr. Appl. Phys. 20:973–981. https://doi.org/10.1016/j.cap.2020.06.005

Bera S, Ghosh D, Dutta A, Bhattacharyya S, Chakraborty S, Pradhan N (2019) Limiting heterovalent B-site doping in CsPbI 3 nanocrystals: phase and optical stability. ACS Energy Lett 4:1364–1369. https://doi.org/10.1021/acsenergylett.9b00787

Bouich A, Ullah S, Marí B, Atourki L, Touhami ME (2021) One-step synthesis of FA1-xGAxPbI3 perovskites thin film with enhanced stability of alpha (α) phase. Mater Chem Phys 258:123973. https://doi.org/10.1016/j.matchemphys.2020.123973

Bouich A, Marí-Guaita J, Baig F, Hameed Khattak Y, Soucase BM, Palacios P (2022) Investigation of the surface coating, humidity degradation, and recovery of perovskite film phase for solar-cell applications. Nanomaterials 12:3027. https://doi.org/10.3390/nano12173027

Bouich A, Torres JC, Chfii H, Marí-Guaita J, Khattak YH, Baig F, Soucase BM, Palacios P (2023) Delafossite as hole transport layer a new pathway for efficient perovskite-based solar sells: insight from experimental, DFT and numerical analysis. Sol Energy 250:18–32. https://doi.org/10.1016/j.solener.2022.12.022

Chen K, Jin W, Zhang Y, Yang T, Reiss P, Zhong Q, Bach U, Li Q, Wang Y, Zhang H, Bao Q, Liu Y (2020) High efficiency mesoscopic solar cells using CsPbI 3 perovskite quantum dots enabled by chemical interface engineering. J Am Chem Soc 142:3775–3783. https://doi.org/10.1021/jacs.9b10700

Dunfield SP, Bliss L, Zhang F, Luther JM, Zhu K, van Hest MFAM, Reese MO, Berry JJ (2020) From defects to degradation: a mechanistic understanding of degradation in perovskite solar cell devices and modules. Adv Energy Mater 10:1904054. https://doi.org/10.1002/aenm.201904054

Fradi K, Bouich A, Slimi B, Chtourou R (2022) Towards improving the optoelectronics properties of MAPbI3(1–x)B3x/ZnO heterojunction by bromine doping. Optik (Stuttg) 249:168283. https://doi.org/10.1016/j.ijleo.2021.168283

Fu Y, Hautzinger MP, Luo Z, Wang F, Pan D, Aristov MM, Guzei IA, Pan A, Zhu X, Jin S (2019) Incorporating large A cations into lead iodide perovskite cages: relaxed Goldschmidt tolerance factor and impact on exciton–phonon interaction. ACS Cent Sci 5:1377–1386. https://doi.org/10.1021/acscentsci.9b00367

Guo Y, Yin X, Liu J, Que W (2019) Highly efficient CsPbIBr 2 perovskite solar cells with efficiency over 9.8% fabricated using a preheating-assisted spin-coating method. J Mater Chem A 7:19008–19016. https://doi.org/10.1039/C9TA03336J

Guvenc CM, Yalcinkaya Y, Ozen S, Sahin H, Demir MM (2019) Gd 3+ -Doped α-CsPbI 3 nanocrystals with better phase stability and optical properties. J Phys Chem C 123:24865–24872. https://doi.org/10.1021/acs.jpcc.9b05969

Huang J, Lei T, Siron M, Zhang Y, Yu S, Seeler F, Dehestani A, Quan LN, Schierle-Arndt K, Yang P (2020) Lead-free cesium europium halide perovskite nanocrystals. Nano Lett 20:3734–3739. https://doi.org/10.1021/acs.nanolett.0c00692

Jeong M, Choi IW, Go EM, Cho Y, Kim M, Lee B, Jeong S, Jo Y, Choi HW, Lee J, Bae JH, Kwak SK, Kim DS, Yang C (2020) Stable perovskite solar cells with efficiency exceeding 24.8% and 0.3-V voltage loss. Science (80-.) 369:1615–1620. https://doi.org/10.1126/science.abb7167

Jeong J, Kim M, Seo J, Lu H, Ahlawat P, Mishra A, Yang Y, Hope MA, Eickemeyer FT, Kim M, Yoon YJ, Choi IW, Darwich BP, Choi SJ, Jo Y, Lee JH, Walker B, Zakeeruddin SM, Emsley L, Rothlisberger U, Hagfeldt A, Kim DS, Grätzel M, Kim JY (2021) Pseudo-halide anion engineering for α-FAPbI3 perovskite solar cells. Nature 592:381–385. https://doi.org/10.1038/s41586-021-03406-5

Khattak YH, Baig F, Shuja A, Beg S, Soucase BM (2020) Numerical analysis guidelines for the design of efficient novel nip structures for perovskite solar cell. Sol Energy 207:579–591. https://doi.org/10.1016/j.solener.2020.07.012

Khattak YH, Baig F, Shuja A, Atourki L, Riaz K, Soucase BM (2021) Device optimization of PIN structured perovskite solar cells: impact of design variants. ACS Appl Electron Mater 3:3509–3520. https://doi.org/10.1021/acsaelm.1c00460

Khattak YH, Vega E, Baig F, Soucase BM (2022) Performance investigation of experimentally fabricated lead iodide perovskite solar cell via numerical analysis. Mater Res Bull 151:111802. https://doi.org/10.1016/j.materresbull.2022.111802

Khattak YH, Baig F, Bouich A, Marí-Guaita J, Shuja A, Soucase BM (2023) Designing next-generation kesterite solar cells: a systematic numerical investigation of innovative structures and design variants for enhanced photovoltaic performance. Sol Energy 265:112105. https://doi.org/10.1016/j.solener.2023.112105

Kim Y-H, Kim S, Kakekhani A, Park J, Park J, Lee Y-H, Xu H, Nagane S, Wexler RB, Kim D-H, Jo SH, Martínez-Sarti L, Tan P, Sadhanala A, Park G-S, Kim Y-W, Hu B, Bolink HJ, Yoo S, Friend RH, Rappe AM, Lee T-W (2021) Comprehensive defect suppression in perovskite nanocrystals for high-efficiency light-emitting diodes. Nat Photonics 15:148–155. https://doi.org/10.1038/s41566-020-00732-4

Kulbak M, Cahen D, Hodes G (2015) How important is the organic part of lead halide perovskite photovoltaic cells? Efficient CsPbBr 3 cells. J Phys Chem Lett 6:2452–2456. https://doi.org/10.1021/acs.jpclett.5b00968

Liu Y, Yang Z, Cui D, Ren X, Sun J, Liu X, Zhang J, Wei Q, Fan H, Yu F, Zhang X, Zhao C, Liu SF (2015) Two-inch-sized perovskite CH 3 NH 3 PbX 3 (X = Cl, Br, I) crystals: growth and characterization. Adv Mater 27:5176–5183. https://doi.org/10.1002/adma.201502597

Lu M, Zhang X, Zhang Y, Guo J, Shen X, Yu WW, Rogach AL (2018) Simultaneous strontium doping and chlorine surface passivation improve luminescence intensity and stability of CsPbI 3 nanocrystals enabling efficient light-emitting devices. Adv Mater 30:1804691. https://doi.org/10.1002/adma.201804691

Lu Y, Wang Q, Chen R, Qiao L, Zhou F, Yang X, Wang D, Cao H, He W, Pan F, Yang Z, Song C (2021) Spin-dependent charge transport in 1D chiral hybrid lead-bromide perovskite with high stability. Adv Funct Mater 31:2104605. https://doi.org/10.1002/adfm.202104605

MaríSoucase B, Baig F, Hameed Khattak Y, Vega E, Mollar M (2022) Numerical analysis for efficiency limits of experimental perovskite solar cell. Sol Energy 235:200–208. https://doi.org/10.1016/j.solener.2022.02.051

McMeekin DP, Sadoughi G, Rehman W, Eperon GE, Saliba M, Hörantner MT, Haghighirad A, Sakai N, Korte L, Rech B, Johnston MB, Herz LM, Snaith HJ (2016) A mixed-cation lead mixed-halide perovskite absorber for tandem solar cells. Science (80-.) 351:151–155. https://doi.org/10.1126/science.aad5845

Mir WJ, Swarnkar A, Nag A (2019) Postsynthesis Mn-doping in CsPbI 3 nanocrystals to stabilize the black perovskite phase. Nanoscale 11:4278–4286. https://doi.org/10.1039/C9NR00248K

Motta C, El-Mellouhi F, Sanvito S (2015) Charge carrier mobility in hybrid halide perovskites. Sci Rep 5:12746. https://doi.org/10.1038/srep12746

Piotrowski M, Ge Z, Wang Y, Bandela AK, Thumu U (2022) Programmable precise kinetic control over crystal phase, size, and equilibrium in spontaneous metathesis reaction for Cs–Pb–Br nanostructure patterns at room temperature. Nanoscale 14:16806–16815. https://doi.org/10.1039/D2NR04102B

Sonmezoglu S, Akin S (2020) Suppression of the interface-dependent nonradiative recombination by using 2-methylbenzimidazole as interlayer for highly efficient and stable perovskite solar cells. Nano Energy 76:105127. https://doi.org/10.1016/j.nanoen.2020.105127

Sun Y, Wu Y, Fang X, Xu L, Ma Z, Lu Y, Zhang W-H, Yu Q, Yuan N, Ding J (2017) Long-term stability of organic–inorganic hybrid perovskite solar cells with high efficiency under high humidity conditions. J Mater Chem A 5:1374–1379. https://doi.org/10.1039/C6TA08117G

Sutton RJ, Eperon GE, Miranda L, Parrott ES, Kamino BA, Patel JB, Hörantner MT, Johnston MB, Haghighirad AA, Moore DT, Snaith HJ (2016) Bandgap-tunable cesium lead halide perovskites with high thermal stability for efficient solar cells. Adv Energy Mater 6:1–6. https://doi.org/10.1002/aenm.201502458

Wang G, Liu J, Lei M, Zhang W, Zhu G (2020) Optimizing the substrate pre-heating and post-annealing temperatures for fabricating high-performance carbon-based CsPbIBr 2 inorganic perovskite solar cells. Electrochim Acta 349:136354. https://doi.org/10.1016/j.electacta.2020.136354

Wang Y, Zhao H, Piotrowski M, Han X, Ge Z, Dong L, Wang C, Pinisetty SK, Balguri PK, Bandela AK, Thumu U (2022) Cesium lead iodide perovskites: optically active crystal phase stability to surface engineering. Micromachines 13:1318. https://doi.org/10.3390/mi13081318

Yadav V, Pandey R, Madan J (2023) CsPbI 3 based perovskite solar cells: ETL parameters optimization using SCAPS-1D. In: 2023 Int. Conf. Smart Syst. Appl. Electr. Sci., IEEE pp. 1–4. https://doi.org/10.1109/ICSSES58299.2023.10200070

Zhao H, Wang Y, Wang C, Bandela AK, Thumu U (2023) Dissolution-dictated recrystallization in cesium lead halide perovskites and size engineering in δ-CsPbI 3 nanostructures. Cryst Growth Des 23:7412–7423. https://doi.org/10.1021/acs.cgd.3c00817

Publisher's Note